# Three-dimensional structure of Cd*X* (*X*=Se,Te) nanocrystals by total x-ray diffraction

S. K. Pradhan[a)]
*Department of Physics, Central Michigan University, Mt. Pleasant, Michigan 48859*

Z. T. Deng and F. Tang
*Technical Institute of Physics and Chemistry, Chinese Academy of Sciences, Beijing 100080, China*

C. Wang
*Key Laboratory of Molecular Engineering of Polymers (Minister of Education), Fudan University, Shanghai 200433, China and Department of Macromolecular Science, Fudan University, Shanghai 200433, China*

Y. Ren
*Advanced Photon Source, Argonne National Laboratory, Argonne, Illinois 60439*

P. Moeck
*Department of Physics, Portland State University, Portland, Oregon 97207*

V. Petkov[b)]
*Department of Physics, Central Michigan University, Mt. Pleasant, Michigan 48859*

(Received 4 April 2007; accepted 25 June 2007; published online 20 August 2007)

The three-dimensional structure of oleic acid-capped CdSe and thiol-capped CdTe nanocrystals used as quantum dots has been determined by total synchrotron radiation x-ray diffraction and atomic pair distribution function analysis. Both CdSe and CdTe are found to exhibit the zinc-blende-type atomic ordering. It is only slightly distorted in CdSe implying the presence of nanosize domains and very heavily distorted in CdTe due to the presence of distinct core-shell regions. The results well demonstrate the great potential of the experimental approach and thus encourage its wider application in quantum dot research. © *2007 American Institute of Physics*.
[DOI: 10.1063/1.2767615]

## I. INTRODUCTION

Semiconductor Me(II)*X*(IV) (*M*=Zn,Cd; *X*=S,Se,Te) nanosize crystals (NCs), also referred to as quantum dots, are being extensively studied due to their unique optical properties finding use in important applications such as biolabeling,[1–4] drug delivery,[5] light emitting diodes,[6] lasers,[7] and solar cells.[8] A major part of this effort is the development of synthetic routes capable of yielding large quantities of Me*X* NCs with a predefined emission energy, high quantum yield, and stability, at low cost. Good progress has been made and now it is already known that the emission energy of Me*X* NCs may be adjusted by tuning their chemical composition, size, and shape.[9,10] It has also been found that the quantum yield and stability may be improved considerably by passivating the NC surface by a thin shell of a higher band gap[11–13] material. It has just been recognized that[14] the optical properties of Me*X* NCs may also be controlled by yet another parameter: the type and symmetry of the atomic arrangement. To explore this opportunity detailed knowledge of the NC three-dimensional (3D) structure is obviously needed. Traditionally the 3D structure of crystals is determined by x-ray diffraction (XRD) experiments, and given in terms of a small number of parameters such as unit cell constants, cell symmetry, and positions of atoms within the unit cell. Semiconductor quantum dots, however, lack the extended order of usual crystals rendering traditional x-ray crystallography very difficult to apply. This has prompted researchers to apply other techniques such as extended x-ray absorption fine structure (EXAFS).[15–17] EXAFS is very sensitive to the first atomic coordination shell but does not provide any information about the longer-range atomic ordering in materials. Besides, structural distortions that often occur in materials structured at the nanoscale often complicate EXAFS analyses.[18] Atomic resolution imaging techniques, such as scanning transmission electron microscopy (STEM), have also been applied.[19,20] STEM images, like any other, are, however, a projection down an axis and may reveal the atomic ordering at the surface of NCs only. The 3D atomic arrangement inside Me*X* NCs that is known to determine many of their bulk properties, including the optical ones, thus remains largely hidden for the spectroscopy and imaging-type techniques currently employed. Here we apply total XRD coupled to atomic pair distribution function (PDF) analysis to determine the 3D structure of Me*X* NCs (Me=Cd; *X*=Se,Te). We demonstrate that this nontraditional approach can reveal the atomic arrangement inside semiconductor NCs in very fine detail and thus merits to be employed in this very active field of research more frequently than now.

[a)]On leave from Department of Physics, The University of Burdwan, Golapbag, Burdwan-713104, West Bengal, India.
[b)]Author to whom correspondence should be addressed; electronic mail: petkov@phy.cmich.edu

 

## II. EXPERIMENT

### A. Sample preparation

A very important class of semiconductor NCs, namely, Cd(Se/Te), was studied. CdSe NCs were produced by a cost-effective and environmentally friendly route, as follows: 20 mmol of CdO, 9.6 ml of oleic acid (OA), and 40 ml of liquid paraffin were mixed in a three-neck flask, and treated at 150 °C until a light yellowish homogeneous solution (hereafter called solution A) was obtained. In another three-neck flask, 1 mmol of Se powder in 50 ml of paraffin was heated to 220 °C until the solution (hereafter called the solution B) turned wine red. About 5 ml of solution A was mixed with solution B, stirred rigorously, and aged at 220 °C. The mixtures were then cooled down to room temperature, washed with methanol, and dried in air at 50 °C. By varying the time of aging CdSe NCs with an average size of 2.5 nm (hereafter called sample 1) and 3.5 nm (hereafter called sample 2) were obtained. Their surface was passivated with oleic acid. CdSe NCs with an average size of ~3 nm (hereafter called sample 3) and a clean (i.e., not OA capped) surface were prepared by leading $H_2Se$ gas into $Cd(NO_3)_2$ solution. More details of the preparation procedure and optical performance of CdSe NCs studied here may be found in Ref. 21.

A well-known route using thioglycolic acid (TGA) was employed to prepare CdTe NCs as follows: NaHTe was first prepared by mixing $NaBH_4$ and Te powder in 2:1 molar ratio in water at 0 °C (hereafter called solution A). 1 mmol of $CdCl_2$ and 1.2 mmol of TGA were dissolved in 50 ml of water. NaOH solution was added to it to dissolve the resulted precipitate and adjust *p*H to 9 (hereafter called solution B). This step was carried out at 4 °C. Solutions A (0.5*M*, 32 $\mu$l) and B (0.02*M*, 4 ml) were mixed, diluted to 40 ml, stirred vigorously, and put into a Teflon-lined stainless steel autoclave with a volume of 50 ml. The autoclave was kept at 180 °C for a preset time period and then cooled to room temperature by a hydrocooling process. Almost monodisperse TGA-capped CdTe NCs with an average size of ~3 nm were obtained in this way. TGA-capped CdTe NCs also showed a very good quantum efficiency (~50%). More details of the preparation procedure and optical performance of CdTe NCs studied here may be found in Refs. 22 and 23.

### B. Transmission electron microscopy

Transmission electron microscopy (TEM) characterization was performed on an FEI Tecnai $G^2$ F20 ST instrument at 200 keV. All samples were prepared by dipping standard carbon-coated Cu grids into the dry nanopowders. Representative high resolution phase contrast TEM images of CdSe and CdTe NCs are shown in Fig. 1.

### C. X-ray diffraction experiments

CdSe (samples 1–3) and CdTe NCs were subjected to XRD experiments at the beamline 11-ID-C (Advanced Photon Source, Argonne National Laboratory) using synchrotron radiation of energy 115.227 keV ($\lambda$=0.1076 Å). Bulk crystalline CdTe was also measured and used as a standard. Synchrotron radiation x rays were employed for two reasons: First, the high flux of synchrotron radiation x rays allowed us to measure the rather diffuse XRD patterns of the NC samples with a greatly improved statistical accuracy. Second, the high energy of synchrotron radiation x rays allowed us to collect data over a wide range (1–30 $Å^{-1}$) of scattering vectors *Q*. Both are an important prerequisite[24,25] to the success of the total XRD/atomic PDF approach employed here. Scattered synchrotron radiation x rays were collected with an imaging plate detector (mar345). Up to ten images were taken from each of the samples. The corresponding images/scans were combined, subjected to geometrical corrections, integrated, and reduced to one-dimensional XRD patterns. Thus obtained XRD patterns of CdSe and CdTe samples are shown in Figs. 2 and 3, respectively.

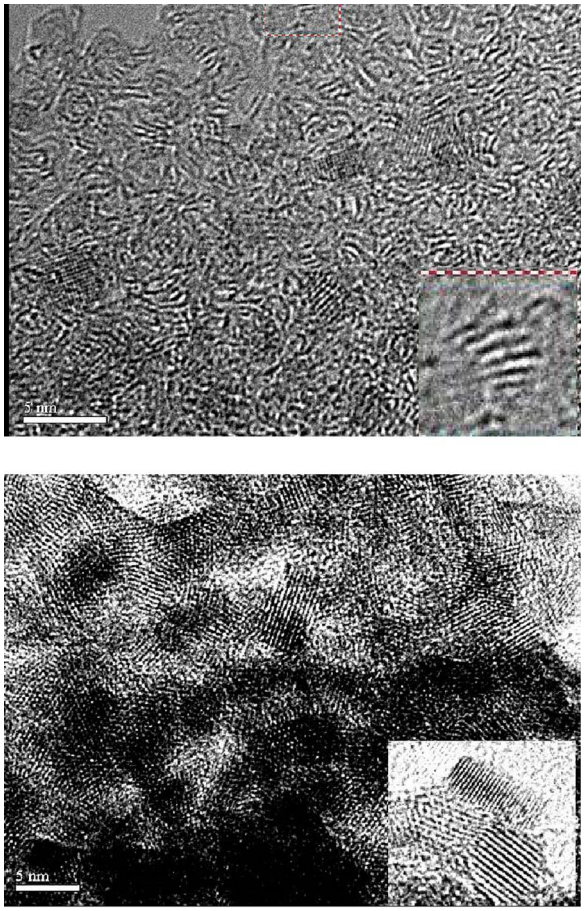


FIG. 1. (Color online) TEM images of OA-capped CdSe (upper image) and TGA-capped CdTe (lower image) NCs. CdSe and CdTe NCs show very good and poor (see the insets) crystallinity, respectively. The length of the bar shown in the images (lower left corner) is 5 nm.

## III. RESULTS

TEM images reveal that most OA route obtained CdSe NCs (only sample 2 shown) are close to spherical in shape and exhibit well-resolved lattice fringes indicating a very good crystallinity. Likely due to its low contrast the OA-capping layer of NCs is not seen.

CdTe NCs too appear rounded in shape (see Fig. 1, lower image). In contrast to CdSe most TGA route obtained CdTe NCs do not exhibit straight and parallel lattice fringes.

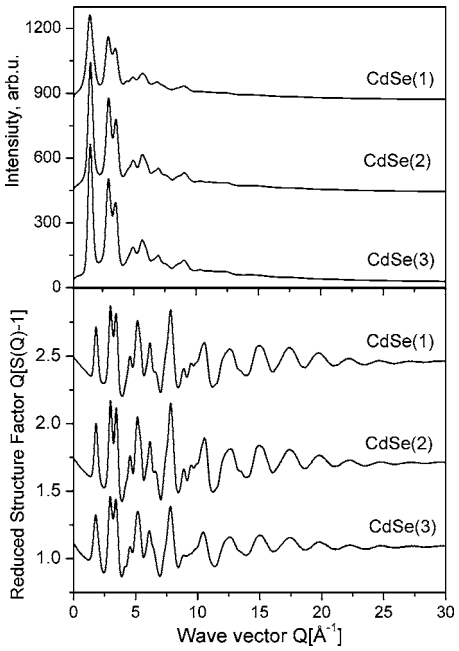


FIG. 2. Synchrotron XRD patterns (upper part) and the corresponding structure factors (lower part) for CdSe NCs.

Instead, lattice fringes (see the inset in Fig. 1, lower image) are bent profoundly indicating the presence of considerable structural distortions. No signature of the TGA-capping layer of NCs is seen either.

As can be seen in Fig. 2 the XRD patterns of CdSe NCs show several well-defined peaks at $Q$ values extending up to $\sim 10$ Å$^{-1}$. The XRD pattern of CdTe NCs (see Fig. 3) shows fewer well-defined peaks again indicating a material of poor crystallinity. Furthermore, the peaks in the XRD patterns of all NCs, CdSe (samples 1–3) and CdTe, are much broader and fewer than those seen in the XRD pattern of a bulk crystal such as the CdTe standard (see Fig. 3). The much

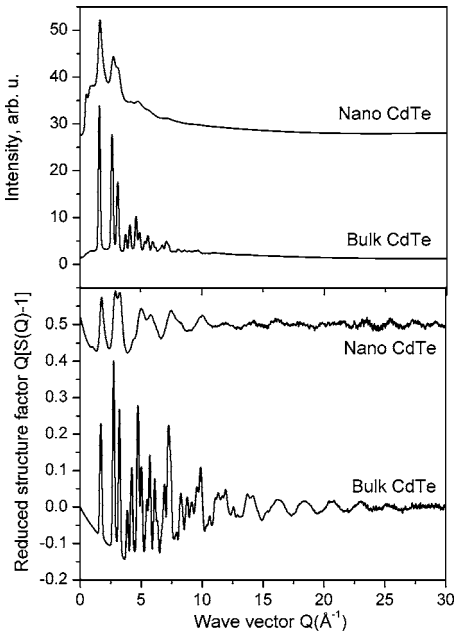


FIG. 3. Synchrotron XRD patterns (upper part) and the corresponding structure factors (lower part) for bulk and NC CdTe.

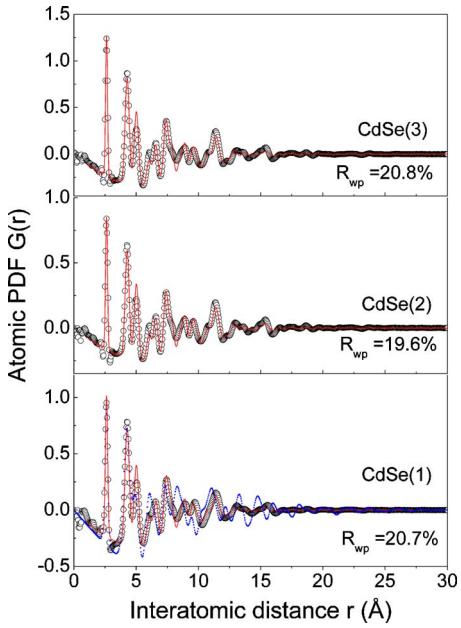


FIG. 4. (Color online) Experimental (open circles) and model (solid line in red) PDFs for CdSe nanoparticles. Model PDFs are based on the zinc blende (cubic) structure with lattice parameters, $a$, of 6.05(1) Å (sample 1), 6.04(1) Å (sample 2), and 6.04(1) Å (sample 3). Agreement (model vs experiment) factors, $R_{wp}$ (Ref. 36), are reported as well. A model PDF based on the wurtzite structure (broken line in blue) is shown as well (the lowest panel).

more diffuse nature and greatly diminished number of well-resolved peaks is indeed what renders the traditional (Bragg) XRD patterns of NCs very difficult to analyze. The problem has its solution in considering all components of the XRD patterns, i.e., the total XRD pattern, in terms of the corresponding atomic PDF. Recently this nontraditional approach has proven to be very successful in structure studies of crystalline materials with substantial structural disorder[24] as well as NCs.[25–27] Structure function $Q[S(Q)-1]$, defined as

$$Q[S(Q)-1] = Q[I^{\mathrm{coh}}(Q) - \sum c_i |f_i(Q)|^2] / |\sum c_i f_i(Q)|^2, \quad (1)$$

where $I^{\mathrm{coh}}(Q)$ is the coherent scattering x-ray intensity per atom in electron units and $c_i$ and $f_i$ are the atomic concentration and x-ray scattering factor, respectively, for the atomic species of type $i$,[25,28,29] are shown in Figs. 2 (for CdSe NCs) and 3 (for CdTe NCs). Their Fourier transforms, the atomic PDFs $G(r)=4\pi r[\rho(r)-\rho_0]$, where $\rho(r)$ and $\rho_0$ are the local and average atomic number densities, respectively, and $r$ is the radial distance are shown in Figs. 4 and 5. The total XRD data processing and derivation of the structure factors and PDFs was done with the help of the program RAD.[30] A comparison between the XRD data and the structure factors extracted from them (see the corresponding data sets presented in Figs. 2 and 3) exemplifies the different way the same diffraction features appear, and hence, are accounted for in traditional (Bragg) and total XRD studies. Traditional XRD patterns are dominated by strong diffraction features at lower Bragg angles (wave vectors) and, hence, are mostly sensitive to longer-range atomic ordering in materials. All diffraction features, including both the sharp (Bragg-

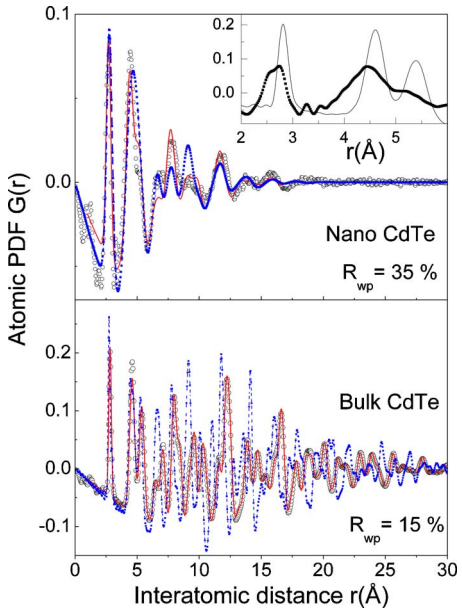


FIG. 5. (Color online) Experimental (open circles) and model (solid line in red) PDFs for bulk and NC CdTe. Agreement (model vs experiment) factors, $R_{wp}$, are reported as well. The low-$r$ peaks in the experimental PDFs for bulk (line) and NC (solid symbols) CdTe are given in the inset on an enlarged scale. Model PDFs (broken line in blue) based on the hexagonal wurtzite structure are shown as well.

like) and diffuselike ones, appear equally strong and are thus all accounted for in the corresponding total structure factors. Thus both the extended (reflected by the Bragg-like scattering) and local (reflected by the diffuselike scattering) structural features of the material under study may be revealed by total XRD coupled to a PDF data analysis. Furthermore, thanks to the properties of Fourier transformation the slow oscillating (diffuselike scattering) components of the total XRD data appear as sharp and, hence, easily identified PDF features in real space enabling convenient testing and refinement of structure models. This greatly enhances the sensitivity to local atomic ordering rendering the Fourier couple $Q[S(Q)-1]$/PDF very well suited to study materials exhibiting a substantially limited length of structural coherence such as nanosize crystals. A few successful PDF studies on semiconductor NCs (Refs. 31 and 32) have already been reported. We push further along this line providing extra evidence for the great potential of total XRD/PDF approach.

## IV. DISCUSSION

Usually bulk CdSe adopts the wurtzite while bulk CdTe the zinc-blende-type structure. Both structure types share the same immediate atomic ordering where each metal (Cd) and nonmetal (Se/Te) atom is tetrahedrally coordinated by unlike atoms. The next nearest and more distant coordination spheres are, however, different in wurtzite and zinc blende. Hence, their crystallographic symmetry is different: cubic in zinc blende and hexagonal in wurtzite. Fragments from the two structure types are shown in Fig. 6. The experimental PDF for bulk CdTe was fitted with models based on the wurtzite and zinc-blende structures. The fit was done with the help of the program PDFFIT.[33] As can be seen in Fig. 5 the zinc-blende-type model reproduces the experimental data in

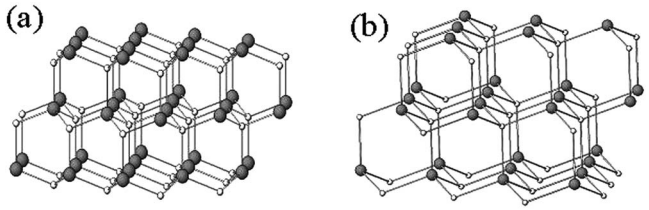


FIG. 6. Fragments from the wurtzite (a) and zinc-blende (b) structures found in bulk Cd(Se/Te). Metal (Cd) and Se/Te are represented as solid and open circles, respectively.

detail while that based on the wurtzite structure fails confirming that atoms in bulk CdTe are arranged on the vertices of a cubic lattice. The PDF refined value of the parameter of that lattice is 6.49(1) Å, which is very close to the literature value of 6.48(1) Å.[34] The result shows that total XRD/PDF analysis is sensitive to the 3D atomic ordering in materials and may be confidently employed in structure search and refinement.

CdTe and CdSe NCs have been reported to adopt either wurtzite or zinc-blende structure, depending on the particular synthetic route employed.[35–38] Both structures were tested against the experimental PDFs for NCs. The tests were done by computing model PDFs and comparing them to the experimental data. The model PDFs were based on literature data (unit cell constants and atomic positions) for the corresponding structure types. The very limited length of structural coherence in the NCs was modeled by multiplying the model PDF data with a decaying exponent as suggested in Ref. 39 and implemented in Ref. 31. The effect of the correction is to depress the PDF uniformly without changing its shape. The calculations were again done with the help of the program PDFFIT. As can be seen in Fig. 4 the experimental PDFs for CdSe NCs may not be reproduced well by a model based on the wurtzite structure. They are, however, very well reproduced by a model based on the zinc-blende structure. This result is another demonstration of the fact that NCs do not necessarily adopt the structure type usually occurring with their bulk counterpart. Here it may be noted that spectroscopy techniques such as EXAFS would have difficulties revealing the symmetry of the atomic ordering in CdSe NCs due to the identical immediate (up to 5 Å; see Fig. 5) atomic ordering in wurtzite and zinc blende. As can also be seen in Fig. 4 all CdSe NCs studied, OA capped (samples 1 and 2) and not OA capped (sample 3), show similar PDFs indicating that the presence of a capping (oleic acid) layer/shell does not affect their atomic ordering substantially. That atomic ordering, however, is not very perfect since the experimental PDFs are seen to decay to zero at interatomic distances of the order of 1.5 nm that are much shorter than the average CdSe NC size (~2.5–3.5 nm) determined by TEM. Differences between XRD and TEM estimates for crystallite size are not uncommon since the former technique is sensitive to the average size of the atomic domains scattering x ray coherently while the latter to the crystal grain size. A crystal, including a NC, may or may not be a single domain object. The fact that the length of structural coherence in CdSe NCs studied is almost half of their "grain" size implies that they are likely to be divided into several, somewhat misoriented with re-

spect to each other atomic domains. The experimental PDF data also show that the parameter of the cubic lattice in CdSe NCs (see data reported in Fig. 4) is slightly contracted with respect to that, $a=6.077(1)$ Å, observed in bulk CdSe.[40] Other semiconductor NCs (Refs. 41 and 42) have shown similar behavior which is believed to be due to a reconstruction of the crystalline lattice at the NC surface.[43–45] Fine structural characteristics such as the presence of internal domain structure and lattice contraction/strain in NCs may not be so straightforwardly identified by spectroscopy techniques either.

As can be seen in Fig. 5 the experimental PDF for CdTe NCs is quite featureless when compared to that of bulk CdTe. It decays to zero faster than the PDFs for CdSe NCs too although both CdSe and CdTe NCs are of very similar size (see TEM in Fig. 1). This indicates that the degree of crystallinity in CdTe NCs is rather low (even lower than that in CdSe NCs). The atomic ordering in CdTe NCs, however, still can be approximated with a periodic, crystalline-type model based on the zinc-blende structure. A model based on the wurtzite structure is not as good an approximation to the NC structure as the results presented in Fig. 5 show. Thus total XRD/PDFs studied allow us to reveal unambiguously the inherent symmetry of atomic ordering in CdTe NCs exhibiting a very poor crystallinity (i.e., a great deal of structural disorder). Traditional XRD studies often fail in similar circumstances. The parameter of the zinc-blende-type (cubic) lattice resulted from the PDF analysis is $a=6.24(1)$ Å, which is much shorter than the lattice parameter of bulk CdTe $a=6.4827$ Å,[46] indicating that CdTe NCs are highly strained too. Furthermore, a careful inspection of the low-$r$ part of the experimental PDF data (see the inset in Fig. 5) shows that, contrary to bulk CdTe, there seem to be two distinct first atomic neighbor distances in CdTe NCs. Note that TEM images do not provide any hint for the existence of two distinct coordination environments in CdTe NCs studied. To reveal the origin of lattice strain and not uniform metal-nonmetal atomic coordination in CdTe NCs we considered two plausible structure models as follows: The first one featured a continuous arrangement of atoms sitting on the vertices of a nonuniformly strained zinc-blende-type lattice. The model may be looked at as an assembly of randomly oriented with respect to each other and quite distorted/strained CdTe clusters (~6.5 Å) merging into a single NC/grain which thus shows a smaller degree of strain on average. Such a structural pattern has been observed in bulk semiconductors[24] as well as in NCs.[27] The model was attempted and refined well [see Fig. 7(b)] to a lattice that is quite contracted locally ($a=6.162$ Å) and much more relaxed ($a=6.294$ Å) at longer-range distances. This model featuring, in essence, a nonuniformly strained but yet a single phase material, however, still could not explain the presence of two distinct first neighbor distances in CdTe NCs [see the inset in Fig. 7(b)]. That is why it was modified to incorporate a mixture of two zinc-blende-type lattices (i.e., to feature a two-phase CdTe NC). Thus modified model performed much better as the results in Fig. 7(a) show. The refined lattice parameters of the two distinct cubic lattices are $a_1=5.724$ Å and $a_2=6.306$ Å. The

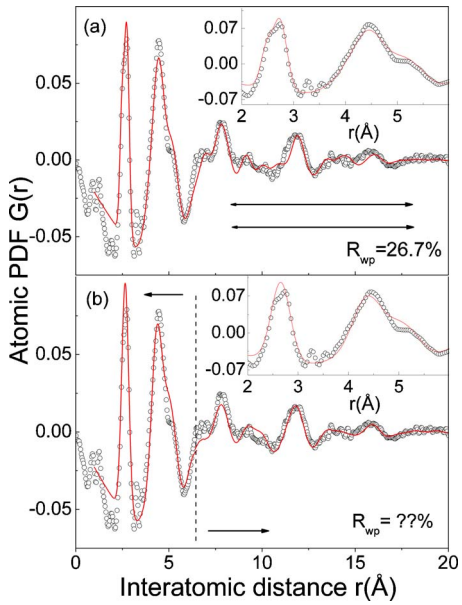


FIG. 7. (Color online) Experimental (open circles) and model (solid line) PDFs for nanoparticle CdTe. Model PDFs are based on (a) mixture of two distinct zinc-blende-type lattices and (b) a single but nonuniformly strained zinc-blende-type lattice with a very contracted local and a more relaxed longer-range atomic ordering. The vertical broken line marks the local/longer-range boundary (~6.5 Å) in that lattice. Agreement (model vs experiment) factors, $R_{wp}$, are shown as well. The low-$r$ peaks in the experimental and model PDFs are given in the insets on an enlarged scale.

result clearly shows that CdTe NCs are indeed a two-phase material, which is not so straightforward to infer from the TEM images alone.

EXAFS experiments[16] on TGA-capped CdTe NCs prepared by others too have identified two distinct Cd-nonmetal distances. The shorter one (~2.5 Å) has been identified as Cd–S and the longer one (~2.8 Å) as Cd–Te distance. The apparent "phase separation" in those CdTe NCs has been explained in terms of a S-rich surface and Te-rich interior. Sulfur is present in TGA molecules ($HS-CH_2CO_2H$) which bind to surface Te sites thus creating fourfold coordinated S atoms, instead of threefold coordinated Te atoms with a dangling bond. This has been shown to improve the photochemical properties of NCs considerably. As pointed out earlier[22,23] some TGA molecules may hydrolyze during the NC preparation and let sulfur atoms diffuse inside NCs creating a gradient of sulfur content close to their surface,[47] i.e., a CdTe/S shell. The presence of CdTe/S shell explains our findings very well: the two distinct zinc-blende-type phases ($a_1=5.724$ Å and $a_2=6.306$ Å) revealed by the PDF analyses are very likely to be a CdS-rich shell and CdTe-rich core. For reference, the lattice parameters of bulk CdS and CdTe are 5.8304 and 6.4827 Å,[46] respectively. Both the core and shell of CdTe NCs seem to be somewhat strained since the lattice parameters of both nanophases differ from those of the corresponding bulk solids in ~0.1 Å. The core and shell in CdTe NCs, however, do not seem to influence each other much since their zinc-blende lattices remain quite distinct (i.e., incoherent; ~0.5 Å difference in their lattice parameters) from each other.

## V. CONCLUSION

Total x-ray diffraction and PDF data analysis can be successfully employed to determine the 3D atomic arrangement in semiconductor NCs including the structure type and symmetry, the degree of crystallinity, presence of strain, sub-NC structure such as atomic domains, and distinct nanophase inhomogeneities (e.g., core/shell). The approach bridges the gap between spectroscopy (sensitive to the first atomic neighbor ordering only) and imaging (yielding mostly NC grain size, morphology, and surface). It provides a quantitative foundation to understanding, predicting, and thus possibly improving the structure-dependent properties of quantum dots further.

## ACKNOWLEDGMENTS

The work was supported by NSF through Grant No. DMR 0304391(NIRT) and CMU through Grant No. REF C602281. Use of the Advanced Photon Source was supported by the U. S. Department of Energy, Office of Science, Office of Basic Energy Sciences, under Contract No. DE-AC02-06CH11357. One of the authors (C.W.) is grateful to the support of National Science Foundation for Distinguished Young Scholars of China (50525310).

[1] M. Bruchez, M. Moronne, P. Gin, S. Weiss, and A. P. Alivisatos, Science **281**, 2013 (1998).
[2] M. Han, X. Gao, J. Z. Su, and S. Nie, Nat. Biotechnol. **19**, 631 (2001).
[3] W. C. W. Chan, D. J. Maxwell, X. Gao, R. E. Bailey, M. Han, and S. Nie, Curr. Opin. Biotechnol. **13**, 40 (2002).
[4] C. A. Leatherdale, W. K. Woo, F. V. Mikulec, and M. G. Bawendi, J. Phys. Chem. B **106**, 7619 (2002).
[5] X. Gao, Y. Cui, R. M. Levenson, L. W. K. Chung, and S. Nie, Nat. Biotechnol. **22**, 969 (2004).
[6] V. L. Colvin, M. C. Schlamp, and A. P. Alivisatos, Nature (London) **370**, 354 (1994).
[7] V. I. Klimov, A. A. Mikhailovsky, S. Xu, A. Malko, J. A. Hollingsworth, C. A. Leatherdale, H. J. Eisler, and M. G. Bawendi, Science **290**, 314 (2000).
[8] N. C. Greenham, X. G. Peng, and A. P. Alivisatos, Phys. Rev. B **54**, 17628 (1996).
[9] X. Peng, L. Manna, W. Yang, J. Wickham, E. Scher, A. Kadavanich, and A. Alivisatos, Nature (London) **404**, 59 (2000).
[10] L. Manna, E. C. Scher, and A. P. Alivisatos, J. Am. Chem. Soc. **122**, 12700 (2000).
[11] B. O. Dabbousi, J. Rodriguez-Viejo, F. V. Mikulec, J. R. Heine, H. Mattoussi, R. Ober, K. F. Jensen, and M. G. Bawendi, J. Phys. Chem. B **101**, 9463 (1997).
[12] M. A. Hines and Ph. Guyot-Sionnest, J. Phys. Chem. **100**, 468 (1996).
[13] X. Peng, M. C. Schlamp, A. V. Kadavanich, and A. P. Alivisatos, J. Am. Chem. Soc. **119**, 7019 (1997).
[14] G. M. Dalpian, M. L. Tiago, M. L. Puerto, and J. R. Chelikovsky, Nano Lett. **6**, 501 (2006).
[15] J. Rockenberger, L. Troger, A. L. Rogach, M. Tischer, M. Grundmann, A. Eychmuller, and H. Weller, J. Chem. Phys. **108**, 7807 (1998).
[16] A. Eychmuller and A. L. Rorach, Pure Appl. Chem. **72**, 179 (2000).
[17] A. C. Carter, C. E. Bouldin, K. M. Kemner, M. I. Bell, J. C. Woicik, and S. A. Majetich, Phys. Rev. B **55**, 13822 (1997).
[18] D. S. Yang, D. R. Fazzini, T. I. Morrison, L. Troger, and G. Bunker, J. Non-Cryst. Solids **210**, 275 (1997).
[19] J. McBride, J. Treadway, L. C. Feldman, S. J. Pennycook, and S. J. Rosenthal, Nano Lett. **7**, 1496 (2006).
[20] J. McBride, T. Kippeny, S. J. Pennycook, and S. J. Rosenthal, Nano Lett. **4**, 1279 (2004).
[21] Z. T. Deng, L. Cao, F. Q. Tang, and B. S. Zou, J. Phys. Chem. B **109**, 16671 (2005).
[22] H. Zhang, L. Wang, H. Xiong, L. Hu, B. Yang, and W. Li, Adv. Mater. (Weinheim, Ger.) **15**, 1712 (2003).
[23] J. Gao, W. Yang, and C. Wang, J. Phys. Chem. B **109**, 17467 (2005).
[24] V. Petkov, I. -K. Jeong, J. S. Chung, M. F. Thorpe, S. Kycia, and S. J. L. Billinge, Phys. Rev. Lett. **83**, 4089 (1999).
[25] T. Egami and S. J. L. Billinge, *Underneath the Bragg Peaks. Structural Analysis of Complex Materials* (Pergamon, Oxford, 2003).
[26] V. Petkov, P. Y. Zavalji, S. Lutta, M. S. Whittingham, V. Parvanov, and S. Shastri, Phys. Rev. B **69**, 085410 (2004).
[27] M. Gateshki, V. Petkov, G. Williams, S. K. Pradhan, and Y. Ren, Phys. Rev. B **71**, 224107 (2005).
[28] H. P. Klug and L. E. Alexander, *X-ray Diffraction Procedures for Polycrystalline Materials* (Wiley, New York, 1974).
[29] Y. Waseda, *The Structure of Nanosrystalline Materials* (McGraw-Hill, New York, 1980).
[30] V. Petkov, J. Appl. Crystallogr. **22**, 387 (1989).
[31] H. Zhang, B. Gilbert, N. Huang, and J. F. Banfield, Nature (London) **424**, 1025 (2003).
[32] R. B. Neder and V. I. Korsunsiy, J. Phys.: Condens. Matter **17**, S125 (2005).
[33] Th. Proffen and S. J. L. Billinge, J. Appl. Crystallogr. **32**, 572 (1999).
[34] M. Kh. Rabadanov, I. A. Verin, Yu. M. Ivanov, and V. I. Simonov, Kristallografiya **46**, 703 (2001).
[35] L. E. Brus, Appl. Phys. A: Solids Surf. **53**, 465 (1991).
[36] It may be noted that the agreement factors achieved with the PDF analyses appear somewhat higher when compared to those usually resulted from the Rietveld analyses of conventional diffraction data in reciprocal space. This reflects the fact that the atomic PDF differs from the conventional XRD pattern being a quantity much more sensitive to the local atomic ordering in materials. As a result, $R_w$'s between 10% and 20% are common for PDF analyses. The inherently higher absolute value of the goodness-of-fit factors resulted from PDF-based analyses does not affect their functional purpose as a residual quantity that must be minimized to find the best fit and as a quantity allowing to differentiate between competing structural models.
[37] H. Weller, Adv. Mater. (Weinheim, Ger.) **5**, 88 (1993).
[38] S. K. Vashist, R. Tewari, R. P. Bajpal, L. M. Bharadwaj, and R. Reiteri, Nanotechnology **2**, 1 (2006).
[39] S. Ergun and S. R. Schehl, Carbon **11**, 127 (1973).
[40] P. D. Lao, Y. Guo, G. G. Siu, and S. C. Shen, Phys. Rev. B **48**, 11701 (1993).
[41] G. Scamarcio, M. Lugara, and D. Manno, Phys. Rev. B **45**, 13792 (1992).
[42] Y. Hwang, S. Shin, H. Park, S. Park, U. Kim, H. Jeong, E. Shin, and D. Kim, Phys. Rev. B **54**, 15120 (1996).
[43] N. Herron, J. Calabrese, W. Farneth, and Y. Wang, Science **259**, 1426 (1993).
[44] Y. Wang and N. Herron, Phys. Rev. B **42**, 7253 (1990).
[45] J.-Yu. Zhang, X.-Yo Wang, M. Xiao, L. Qu, and X. Peng, Appl. Phys. Lett. **81**, 2076 (2002).
[46] D. Rodic, V. Spasojevic, A. Bajorek, and P. Oennerud, J. Magn. Magn. Mater. **152**, 159 (1996).
[47] H. Borchert, D. V. Talapin, N. Gopanik, C. McGinley, S. Adam, A. Lobo, T. Moller, and H. Weller, J. Phys. Chem. B **107**, 9662 (2003).